LIMNOLOGY
and
OCEANOGRAPHY: METHODS

ASLO

Limnol. Oceanogr.: Methods 16, 2018, 339–355

doi: 10.1002/lom3.10251

Embedding and slicing of intact in situ collected marine snow

Clara M. Flintrop,[1,2*] **Andreas Rogge**,[1] **Sebastian Miksch**,[3] **Stefan Thiele**,[4] **Anya M. Waite**,[1,5] **Morten H. Iversen**[1,2*]

[1]Alfred Wegener Institute for Polar and Marine Research, Bremerhaven, Germany
[2]MARUM and University of Bremen, Bremen, Germany
[3]Max-Planck-Institute for Marine Microbiology, Bremen, Germany
[4]Institute for Inorganic and Analytical Chemistry, Friedrich Schiller University, Jena, Germany
[5]FB2 Chemistry/Biology, University of Bremen, Bremen, Germany

Abstract

The biological carbon pump is largely driven by the formation and sinking of marine snow. Because of their high organic matter content, marine snow aggregates are hotspots for microbial activity, and microbial organic matter degradation plays an important role in the attenuation of carbon fluxes to the deep sea. Our inability to examine and characterize microscale distributions of compounds making up the aggregate matrix, and of possible niches inside marine snow, has hindered our understanding of the basic processes governing marine carbon export and sequestration. To address this issue, we have adapted soft-embedding and sectioning to study the spatial structure and components of marine aggregates at high resolution. Soft-embedding enables rapid quantitative sampling of undisturbed marine aggregates from the water column and from sediment traps, followed by spatially resolved staining and characterization of substrates of the aggregate matrix and the microorganisms attached to it. Particular strengths of the method include in situ embedding in sediment traps and successful fluorescence in situ hybridization (FISH)-probe labeling, supporting studies of microbial diversity and ecology. The high spatial resolution achieved by thin-sectioning of soft-embedded aggregates offers the possibility for improved understanding of the composition and structure of marine snow, which directly influence settling velocity, microbial colonization and diversity, degradation rates, and carbon content. Our method will help to elucidate the small-scale processes underlying large-scale carbon cycling in the marine environment, which is especially relevant in the context of rising anthropogenic CO_2 emissions and global change.

The world's oceans play a key role in the global carbon cycle because of their capacity to act as active carbon sinks (Passow and Carlson 2012; Ciais et al. 2014). There is an annual flux of 80 Pg C from the atmosphere to the ocean, of which 0.1 Pg C are exported to the deep sea where carbon is sequestered over timescales of $\geq 10^3$ yr (IPCC 2013). A central mechanism modulating marine carbon sequestration is the large-scale export of organic matter to the dark ocean via the Biological Carbon Pump: phytoplankton fix dissolved inorganic carbon through photosynthesis and, upon sinking, remove carbon from the euphotic zone in the form of particulate organic carbon (POC). Vertical carbon flux is dominated by zooplankton fecal pellets and aggregated organic matter, which together result in an estimated flux of ~ 0.04 Pmol C yr^{-1} (Honjo et al. 2008). Once aggregates are larger than 500 μm in diameter they are collectively called "marine snow" (Alldredge and Silver 1988). Zooplankton grazing and microbial degradation of marine snow are largely responsible for the attenuation of carbon flux to the deep sea, respiring and consuming $\geq 97\%$ of carbon fixed in the surface ocean (Turner 2015).

Despite the important role of marine snow in the marine carbon cycle, the in situ processes and mechanisms underlying colonization and degradation by heterotrophic microorganisms on a sub-aggregate level are relatively unexplored. There are two main reasons for this: (1) the difficulty of sampling undisturbed particles in situ, particularly at depths in the water column where aggregate collection by scuba diving is not possible, and (2) their intricate three-dimensional (3D) structure and composition, which create a heterogeneous habitat with several micro-niches. As a result, microbial colonization and degradation vary in space and intensity both

*Correspondence: clara.flintrop@awi.de; morten.iversen@awi.de

Additional Supporting Information may be found in the online version of this article.

Table 1. Oligonucleotide probes used in this study with specified target organism, oligonucleotide sequence, formamide (FA) concentration in hybridization buffer, and FISH method(s) the probe was used with (mono-FISH, CARD-FISH and/or Mil-FISH).

Probe	Target	Sequence (5′–3′)	FA (%)	FISH method
EUB338	Most bacteria	GCTGCCTCCCGTAGGAGT	35	mono, CARD, MiL
EUB II	Planctomycetes	GCAGCCACCCGTAGGTGT	35	mono, CARD, MiL
EUB III	Verrucomicrobiales	GCTGCCACCCGTAGGTGT	35	mono, CARD, MiL
CF319a	Bacteroidetes	TGGTCCGTGTCTCAGTAC	35	CARD
ALT1413	Alteromonas/Colwellia	TTTGCATCCCACTCCCAT	40	CARD
SYN405	Synechococcus	AGAGGCCTTCATCCCTCA	30	CARD
NON338	Control	ACTCCTACGGGAGGCAGC	35	mono, CARD, MiL

between and within aggregates, and information about biogeochemical processes and microbial interactions is lost without the means to study marine snow at sub-aggregate resolution. Solid, dense material regularly makes up less than 1% of the aggregate volume (Ploug et al. 2008) and consists of a variety of organic and inorganic matter including phytoplankton, fecal pellets, phyto- and zoo-detritus, and ballasting minerals like airborne dust, biominerals, and silt from glaciers (Alldredge and Silver 1988; Ransom et al. 1998; Van der Jagt et al. 2018). How tightly these solids are packed affects the porosity of marine snow, which in turn affects settling behavior and carbon remineralization (Ploug et al. 2008; Iversen and Ploug 2010). In addition to the solid fraction, marine aggregates contain high amounts of extracellular polymeric substances (EPS) including transparent exopolymer particles (TEP). TEP are defined as discrete particles that consist predominantly of surface-active acidic polysaccharides and are stained by Alcian Blue (Alldredge et al. 1993). They can exert significant control over carbon export due to their sticky nature and molecular composition, which influence aggregation dynamics and aggregate buoyancy (Mari et al. 2017). TEP have also been proposed to render aggregates impermeable due to clogging of aggregate pore space (Ploug and Passow 2007). While there is a widely used method to quantify TEP spectrophotometrically (Passow and Alldredge 1995), no method currently exists to assess the spatial distribution and extent of pore space reduction and clogging caused by different fractions of EPS.

Organic matter distribution and quality are tightly interlinked with microbial colonization of aggregates. Bacterial abundance, diversity, enzymatic activity, and carbon respiration per volume aggregate are higher than in the surrounding water column due to increased substrate availability (Alldredge and Gotschalk 1990; DeLong et al. 1993; Smith et al. 1992; Ploug and Grossart 2000; D'Ambrosio et al. 2014). Krupke et al. (2016) showed how quorum sensing can regulate enzymatic activity and POC degradation in sinking aggregates, suggesting that the positioning and connectivity of microbial clusters within aggregates is an important determinant of microbial activity. This further corroborates the importance of studying the spatial distribution of solid material and EPS/TEP, especially in relation to the localization of heterotrophic microorganisms, to better understand the microbial ecology and small-scale degradation dynamics of marine snow. Advances in the in situ collection of marine snow, e.g., by using a Marine Snow Catcher (MSC; Riley et al. 2012) or sediment traps containing gel-filled collection cups (first proposed by Lundsgaard 1995), have made it possible to non-destructively sample individual aggregates, but the spatial distribution of matter and cells inside aggregates remains obscure without the means to preserve their 3D structure during staining and microscopy.

Published works exploring aggregates that were structurally preserved include studies of the structure and colonization of resin-embedded, microtome-sectioned marine aggregates using Transmission Electron Microscopy (Heissenberger et al. 1996; Leppard et al. 1996), confocal laser scanning microscopy (CLSM) of whole marine aggregates (Holloway and Cowen 1997; Waite et al. 2000), riverine aggregates (Neu 2000; Böckelmann et al. 2002) and microtome-sectioned sludge aggregates (Chu et al. 2004), and cryosectioning of riverine aggregates (Luef et al. 2009a,2009b). To study the 3D structure of marine snow with special regard to the localization of matrix components and microbial colonizers, we have developed cryosectioning of gel-embedded, in situ collected marine snow. This approach is suited for rapid subsampling of aggregates collected in situ using sediment trap gels, and for probing of aggregates with bioactive markers such as FISH. We present a modular workflow that enables spatially resolved visualization of individual aggregates and their components, and will advance the study of small-scale processes governing microbial assemblages in marine snow and their connection to carbon cycling in the marine environment.

Materials and procedures

The workflow is divided into (1) aggregate collection, (2) aggregate embedding and sectioning, (3) visualization and imaging of the aggregate matrix, including staining of EPS, 3D-reconstruction, and assessment of aggregate porosity, and (4) visualization of aggregate colonizers, including nucleic

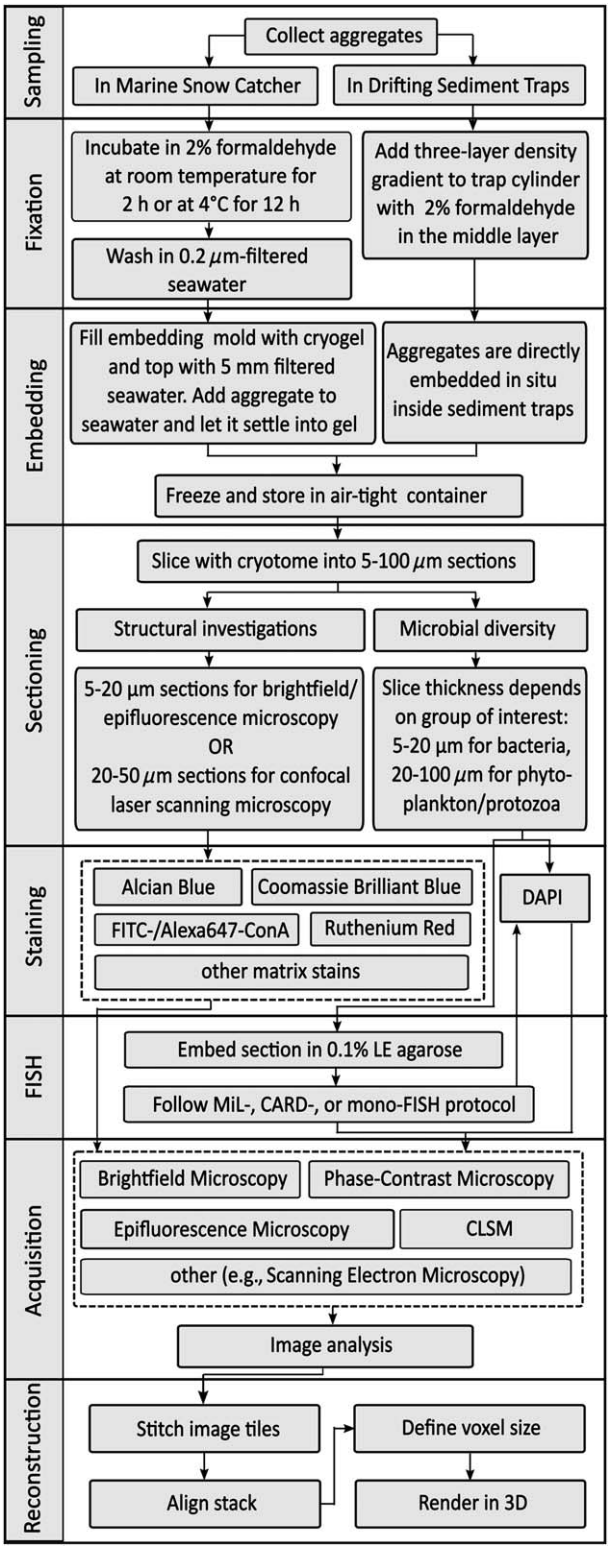

Fig. 1. Work flow of soft-embedding method. Boxes framed by dashed lines denote a "mix-and-match" process depending on the targeted substrate and the required imaging technique. The order in which staining and FISH are carried out depends on the FISH method used. Please refer to "Materials and procedures" section for details.

acid (DAPI) staining and probing of selected bacterial clades using FISH. Please refer to the accompanying flow chart (Fig. 1) for a step-by-step breakdown of the procedures involved.

Sample collection

Samples were collected during the research cruises POS495 and POS508 (RV *Poseidon*) to Cape Blanc, Mauretania in 2016/2017, and DY050 (RRS Discovery) to the Porcupine Abyssal Plain observatory in 2016, using a Marine Snow Catcher and free-drifting sediment traps containing gel-filled collection cups. The MSC was lowered to a chosen depth and closed using a drop weight. Back on deck, aggregates contained in the 100 L volume of seawater were left to settle for any desired amount of time ($\leq$ 2 h for fast-settling particles, longer for a broader range of particles). Hereafter, the water in the top part of the MSC was gently drained and the base of the MSC containing the sedimented aggregates was removed.

For passive handling and to collect samples over depth and time, drifting sediment traps containing gel-filled collection cups were deployed (Fig. 2a). Prior to deployment, one 1 m-long trap cylinder per depth was fitted with a collection cup containing 200 ml of frozen Tissue-Tek® O.C.T.™ Compound (Sakura FineTek; from here on referred to as "Tissue-Tek" or "cryogel") (Wiedmann et al. 2014; Thiele et al. 2015). Tissue-Tek is a viscous transparent cryogel and was selected as the embedding medium to allow a slow diffusive exchange of pore water with the cryogel during settling. To allow for analysis of the microbial community with FISH, a three-layer salinity gradient containing 2% v/v formaldehyde solution (diluted from 37% formaldehyde solution with filtered seawater) in the middle layer was added to each tube by dissolving different concentrations of sodium chloride (2‰, 4‰, or 6‰) in GF/F filtered seawater (*see* Thiele et al. 2015 for a detailed description of the in situ fixation method). The cylinders were suspended gyroscopically at depths of 100 m, 200 m, and 400 m, and any aggregates settling directly into the trap cylinders were first fixed with 2% formaldehyde, then washed in the lower and densest water layer before they settled into the gel, where they were recovered after 24 h (Fig. 2b). Prior to removing the gel cup, aggregates contained in the trap cylinder were left to settle for 6–12 h (depending on the height of the trap tube) to ensure that slow-settling particles would also be embedded in the gel. Gel cups were photographed at high magnification (Fig. 2c,d) and stored at −20°C until further processing.

Embedding and slicing

Aggregates picked from the detached base of the MSC were transferred to a disposable embedding mold (22 × 22 × 20 mm) containing Tissue-Tek with a wide-bore pipette. To maximize structural preservation, aggregates were not added directly to the gel, but to an approximately 5 mm thick layer of filtered seawater added on top, and left to settle into the

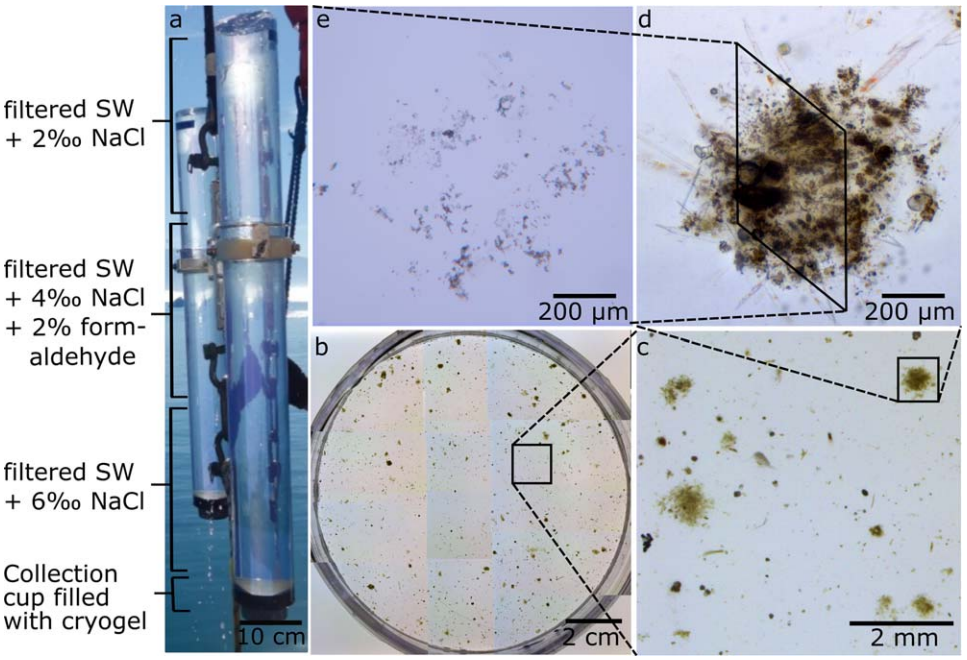

Fig. 2. Collecting and embedding marine snow in situ (counter-clockwise). (**a**) annotated sediment trap cylinder (SW = seawater; NaCl = sodium chloride); (**b**) top view of gel collection cup with in situ embedded aggregates; (**c**) close-up of the gel cup; (**d**) microscopic image of gel-embedded aggregate; (**e**) 10 μm thin-section of in situ embedded aggregate.

gel. Prior to freezing, the position of the aggregate was marked to facilitate the localization of the sample when mounted on the cryotome.

Aggregates embedded in situ in the drifting traps were cut out directly from the frozen collection cup using a small corer. The frozen embedded samples were mounted on a CM-3050S cryostat (Leica Biosystems). Knowing the position of the embedded aggregate, the block containing the sample was cut to size with a razor blade for better handling. Using an object temperature of −30°C and a chamber temperature of −35°C, samples were cut into sections ranging from 5 μm to 100 μm (Fig. 2e). Immediately after cutting, sections were mounted on Superfrost™ Plus slides (ThermoFisher Scientific) and stored at 4°C for short-term processing (within weeks) or at −20°C for longer-term storage (months to years). For microscopic examination, sections were embedded in mounting medium made up of 80% (v/v) Citifluor AF1 (Electron Microscopy Sciences) and 20% (v/v) Vectashield (Vector Laboratories) and covered with a cover slip (ThermoFisher Scientific). The cover slip was sealed with nail polish to avoid smearing the underlying sample.

Visualization and imaging of the aggregate matrix

Staining of EPS

To visualize the EPS matrix, we stained aggregate sections with dyes commonly used for marine snow such as Alcian Blue and Coomassie Brilliant Blue and tested dyes targeting different EPS fractions, including Ruthenium Red, Periodic Acid Schiff-base stain, and the fluorophore-conjugated lectin stain Concanavalin A. Acidic polysaccharides were stained with 0.2 μm-filtered 0.02% Alcian Blue (Sigma-Aldrich) dissolved in 0.06% (v/v) acetic acid (pH 2.5) for 5 s and washed with ultrapure water (UPW; Passow and Alldredge 1995; Long and Azam 1996). A-mannopyranosyl- and α-glucopyranosyl residues of other EPS fractions were targeted with Concanavalin A conjugated with FITC (FITC-ConA; Sigma-Aldrich) or Alexa647 (Alexa647-ConA; Life Technologies) dissolved in 0.3% NaCl was tested at concentrations ranging from 100 μg/mL to 1000 μg/mL (after Uthicke et al. 2009). Proteinaceous particles were stained with Coomassie Brilliant Blue (Sigma-Aldrich). Proteins were stained with 0.2 μm-filtered 0.04% (w/v) Coomassie Brilliant Blue G-250 dissolved in UPW (pH 7.4) for 30 s and washed with UPW (Passow and Alldredge 1995; Long and Azam 1996). Glycosaminoglycans were stained with 0.05% (w/v) Ruthenium Red (Sigma-Aldrich) dissolved in UPW for 10 min followed by washing with UPW (Tiessen and Stewart 1988), and with a Periodic Acid-Schiff kit (Sigma-Aldrich) following the protocol enclosed. Briefly, sections were stained with Periodic Acid Solution for 5 min, with Schiff's reagent for 15 min and counterstained with Hematoxylin Solution, Gill No. 3, for 90 s including intermediate washing steps with UPW.

All stains were applied to untreated sections as well as to sections embedded in 25 μL 0.1% LE agarose prior to staining to test if agarose-embedding can minimize sample loss, as reported for filtered samples. (N.B. in this study, "agarose-embedding" refers to applying a drop of agarose to the sample, and must not to be confused with embedding of intact whole aggregates in agarose).

Aggregate porosity

For a direct, optical measure of porosity (from here on referred to as "optical porosity"), thin-sections were photographed at 200X magnification with phase-contrast microscopy. In addition to in situ collected marine snow, we also examined the optical porosity of marine snow formed in the laboratory from cultures of the diatom *Skeletonema marinoi* to compare porosity between structurally complex, in situ collected aggregates and homogeneous aggregates formed from a monoculture (*see* Iversen and Ploug 2013 for a detailed protocol of diatom culturing and marine snow formation). To assess the reduction of pore space caused by EPS, aggregates were stained with combinations of Alcian Blue, Ruthenium Red, and FITC-ConA/Alexa647-ConA (please refer to "Staining of EPS" for a detailed staining protocol). Alcian Blue and Ruthenium Red-stained sections were photographed at 200X magnification using a light microscope. FITC-ConA/Alexa647-ConA stained sections were imaged at 200X magnification with an epifluorescence microscope (FITC Ex/Em 490 nm/525 nm; Alexa647 Ex/Em 590 nm/617 nm).

All images where processed with the image processing software package FIJI/ImageJ (Schindelin et al. 2012, 2015; Schneider et al. 2012). Images of partial sections ("tiles") were stitched with the FIJI TrakEM2 plug-in (Saalfeld et al. 2010, 2012; Cardona et al. 2012). For processing, images were converted to 8-bit and a threshold value was chosen to separate the aggregate from the background. To measure optical porosity, the area of the solid or stained fraction was measured using the "Analyze Particles" function in ImageJ, divided by the total area of the section and the quotient subtracted from 1. Optical porosity was then compared (1) to the most commonly used method of calculating porosity, where porosity is indirectly inferred from aggregate volume, solid hydrated density, and dry weight (Alldredge and Gotschalk 1988); (2) between and across sections of the same aggregate to assess the distribution of pore space within individual aggregates; (3) between sections of stained and unstained aggregates to assess the respective contributions of selected EPS fractions to changes in porosity.

3D-reconstruction

Two fully sectioned aggregates were selected for 3D reconstruction: one Alcian Blue-stained aggregate sectioned into 50 slices of 10 μm thickness, of which 46 were successfully recovered for alignment; and one unstained aggregate that had been incubated with fluorescently labeled bacteria and was sectioned into 38 sections of 10 μm thickness, of which 35 were successfully recovered. Recovered sections were photographed at 200X magnification using light or epifluorescence microscopy. Image tiles were stitched using the FIJI TrakEM2 plug-in followed by alignment of stitched tiles of consecutive sections in the z-direction using the same plug-in. Sections were aligned based on the positioning of Alcian Blue-stained or green fluorescent material. The aligned sections were exported and rendered in 3D using the 3D viewer plug-in in ImageJ (Schmid et al. 2010).

Visualization of aggregate colonizers

DAPI staining

To visualize microbial cells, cryosections were stained with 1 μg/mL 4′,6-diamidino-2-phenylindole (DAPI) for 10 min at room temperature in the dark. After careful rinsing with UPW, sections were air-dried and embedded in mounting medium for microscopic identification. Alternatively, 1% (v/v) DAPI solution (100 μg/mL) was added directly to the embedding medium. DAPI-stained cells were imaged with epifluorescence or confocal laser scanning microscopy (DAPI Ex/Em 358 nm/461 nm).

Fluorescence in situ hybridization (FISH)

For a more targeted identification of different bacterial groups, we used existing protocols for mono-labeled fluorescence in situ hybridization (mono-FISH), catalyzed reporter deposition fluorescence in situ hybridization (CARD-FISH; Amann et al. 1990; Pernthaler et al. 2002) and multi-labeled fluorescence in situ hybridization (MiL-FISH; Schimak et al. 2015) for staining aggregate thin-sections on glass slides (see Table 1 for a list of organisms targeted in this study and their corresponding oligonucleotide probes). Prior to staining, sections were circled with a hydrophobic PAP pen (Sigma-Aldrich) to retain buffer solutions. Sections were embedded in 25 μL 0.1% low-melting point agarose to maximize structural preservation. For mono- and multi-labeled FISH, hybridization buffer (5M NaCl, 1M TrisHCl, 20% SDS, formamide) with 50 ng/μL probe at a ratio of 15 : 1 was applied followed by hybridization at 46°C for 2 h and subsequent washing at 48°C for 15 min with the adjusted washing buffer (5M NaCl, 1M Tris/HCl, 20% SDS, 0.5M EDTA). For CARD-FISH, thin-sections were treated with lysozyme (50 mg lysozyme dissolved in 500 μL 0.5M EDTA + 500 μL 1M Tris/HCl + 4 mL UPW) for 30–60 min at 37°C for cell wall permeabilization. Hybridization buffer (900 mM NaCl, 20 mM Tris-HCl (pH 7.5), 0.02% sodium dodecyl sulphate (SDS), 10% dextran sulphate (w/v) and 1% (w/v) Blocking Reagent) was mixed with the probe at a buffer : probe ratio of 300 : 1 and applied to the sample. Hybridization at 46°C for 3 h was followed by a subsequent 10 min wash step at 48°C with the adjusted washing buffer (14–900 mM NaCl, 20 mM Tris/HCl, pH 8, 5 mM EDTA, pH 8 and 0.01% SDS). Amplification buffer ($\times$1 PBS [pH 7.3], 0.0015% [v/v] H_2O_2, 1% Alexa Fluor 488 or 594 dye ThermoFisher Scientific, Waltham, Massachusetts, U.S.A.) was prepared and slides incubated for 1 h at 46°C in a humid chamber until a final wash for 10 min in $\times$1 PBS. After washing, sections were incubated with a 1 μg/mL DAPI solution for 5–10 min at room temperature in the dark, washed with UPW, air-dried and embedded with 4 : 1 Citifluor/Vectashield mounting medium. Mounted samples were imaged with an epifluorescence microscope

(Ex/Em 490 nm/525 nm for FITC-labeled probes or tyramides, Ex/Em 358 nm/461 nm for CY3-labeled probes or tyramides).

Assessment

Embedding and slicing

We assessed the feasibility of aggregate embedding and thin-sectioning based on criteria relating to the direct ease of the procedure, the cost and time involved, and the quality of the sections obtained. Embedding of marine snow in Tissue-Tek was a fast and simple process. All aggregates collected from the MSC for this study were ballasted enough to sink into the cryogel within less than 1 h. Moreover, aggregates embedded in situ were spread evenly across the collection cup, enabling clear differentiation between aggregate types before slicing (Fig. 2b,c). Close examination showed very good structural preservation of gel-embedded aggregates with intact pigments and clearly identifiable components, e.g., diatoms protruding from the center of the aggregate (Fig. 2c,d). To avoid gradual dehydration of the Tissue-Tek during frozen storage, we recommend leaving a layer of 0.2 μm-filtered seawater on top of the gel and placing the frozen embedded samples in air-tight bags. During thawing, the relatively higher density of the cryogel prevents mixing with the water layer, which can be removed gently before the gel is re-frozen, mounted, and sectioned.

Tissue-Tek embedded marine snow was successfully sectioned with a mounting efficiency of 90% ($\pm$ 10%). The material properties of Tissue-Tek permitted cutting sections between 5 μm and 100 μm in thickness, which enabled spatially resolved examination of organisms and structures spanning two orders of magnitude. Sections below 5 μm were prone to rupturing, probably because the supporting embedding matrix was not rigid enough to allow structurally preserved slicing of ultra-thin sections. Sections thicker than 100 μm on the other hand were prone to breaking during sectioning because of the rigidity of frozen cryogel. Thick sections ($>$ 50 μm) yielded optimal results when studying the distribution of larger organisms such as phytoplankton cells or flagellates within an aggregate, or in conjunction with CLSM, where optical sectioning of nano- to micrometer-thick slices can be combined with cryotome-sectioning to reduce physical disturbance. However, Tissue-Tek is liquid (albeit highly viscous) at room temperature and in sections thicker than 50 μm the gel was observed to spill over the original boundaries of the section after thawing, resulting in flattening and possible distortion of the 3D structure. Therefore, we recommend a section thickness of 50–100 μm when studying larger organisms, and a section thickness of 5–50 μm for porosity measurements and reconstruction of the aggregate matrix.

Other possible artifacts introduced through slicing include smearing of the sample due to high amounts of silica and lithogenic material found in marine snow which can break along fault lines or be dragged across the section, resulting in the displacement and rupture of material. While this is a potentially strong contraindication against soft-embedding, we did not observe smearing in sections thicker than 5 μm and successfully reconstructed entire aggregates in three dimensions from thin-sections (*see* "3D-reconstruction" section). Optionally, cutting relatively thick sections ($>$ 30 μm) combined with optical sectioning using CLSM can be used to obtain high depth resolution while avoiding smearing. The freezing process during soft-embedding has also been reported to cause damage, mainly through tissue rupturing due to ice crystal formation (Tokuyasu 1973). Ice crystal formation can be minimized through freezing at -80°C or snap-freezing in liquid nitrogen, although no freezing artifacts were observed in cryosections of marine snow frozen at -20°C, possibly due to loose connectivity of the solid fraction and thorough infiltration of pore space by the cryogel.

Soft-embedding and cryosectioning required low-cost consumables, and costs could be reduced further by using non-coated glass slides, applying a coating, or only mounting every n^{th} section of the aggregate, depending on the purpose of sectioning. We conclude that due to easy manipulation and mounting of frozen embedded samples and high recovery efficiency of sections, soft-embedding is a feasible tool for users with little to no previous experience with thin-sectioning.

Visualization and imaging of the aggregate matrix

Staining of the aggregate matrix was assessed based on the coverage and visibility of the stain, the compatibility with cell stains, the compatibility with soft-embedding, and the comparison to whole-aggregate staining. Generally, any stain applicable to aggregates filtered as a whole could also be used on aggregate sections. Concerning the brightness and visibility of any stain, the issue of strong autofluorescence of aggregate components applied here as much as it has been noted to be a problem for whole aggregate examination (Fig. 3; Woebken et al. 2007; Thiele et al. 2015).

When using fluorescent stains, we found that examining sections prior to staining helped with selecting a suitable stain with little overlap in the spectrum of autofluorescent material. We observed the highest amount of autofluorescence to be emitted in the green spectrum, while autofluorescence was weakest in the blue, red and deep red spectra. However, this may change according to aggregate composition and is highly dependent on organic matter quality, as e.g., chlorophyll *a* emits red fluorescence and was observed to have high fluorescent intensities in laboratory-formed aggregates containing healthy, active diatom cells, but not in in situ collected marine snow.

Staining of EPS

Alcian Blue successfully stained TEP of the aggregate matrix (Fig. 4a–c), as previously reported for whole, filtered

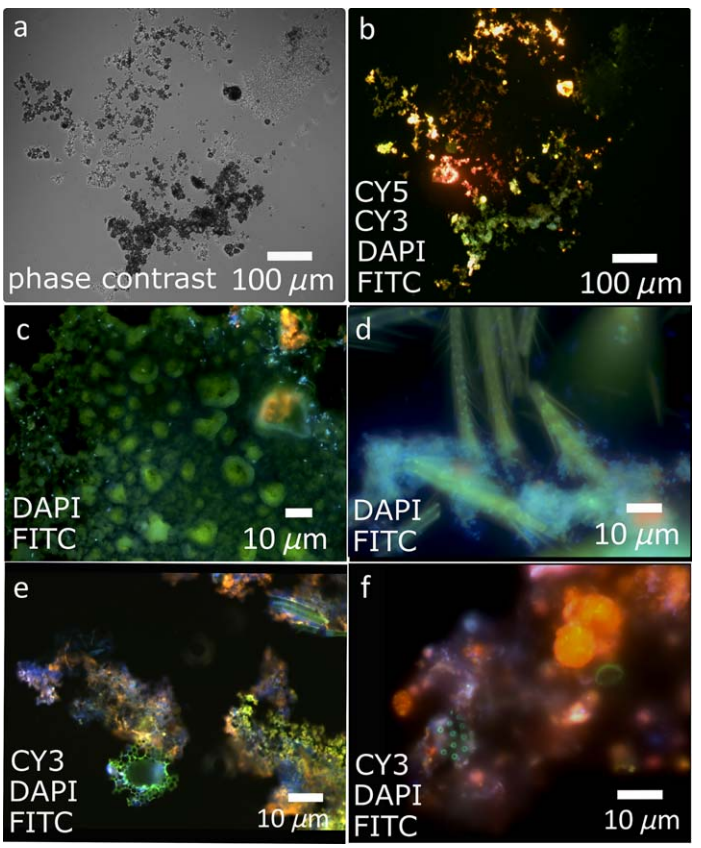

Fig. 3. Autofluorescent matrix components of unstained aggregate sections. (**a**) phase-contrast image of 10 μm-thick section; (**b**) the same section imaged with fluorescence microscopy; (**c**) unidentified structure with sparse bacterial attachment (DAPI-stained cells in blue); (**d**) heavy colonization of copepodide legs by DAPI-stained bacteria (blue); (**e**, **f**) unidentified structures.

marine snow (Passow and Alldredge 1995; Cisternas-Novoa et al. 2015). Coomassie Brilliant Blue staining yielded visible but weak signals of CSP and we observed CSP to be considerably less abundant than TEP, if not completely absent, which could be explained by the higher solubilization of proteins compared to polysaccharides in marine snow (Smith et al. 1992). FITC-ConA and Alexa647-ConA also successfully stained the aggregate matrix at concentrations as low as 100 μg/mL (Figs. 4d, 7), which was expected as lectin stains have been explored in considerable depth for staining EPS in biofilms (Neu et al. 2001; Strathmann et al. 2002), river snow (Neu 2000; Böckelmann et al. 2002), and sludge aggregates (McSwain et al. 2005; Weissbrodt et al. 2013). Compared to Alcian Blue, FITC-ConA/Alexa647-ConA covered similar areas of the aggregate matrix but stained slightly distinctive features. A similar observation was made for Ruthenium Red (Fig. 4). All three stains partially overlapped in their specificity for certain polysaccharides, but also bound to substrates not targeted by any of the other tested stains, highlighting the necessity to further explore polysaccharide diversity and their respective effects on particle aggregation (their "stickiness"), pore space reduction and degradation dynamics.

Special attention must be paid to avoid sample loss during rigorous staining or washing because of the solubility of cryogel in water. The SuperFrost Plus^{TM} coating of the glass slides used in this study is designed to confer maximum samples adherence, but there is a risk of material being washed off, especially of thicker sections where material is not in direct contact with the adhesive coating of the slide. Decreased adhesion was seen in sections that had been stored for >1 yr, meaning that swift processing of sections is advisable. We found that carefully applying the staining or washing solution with a pipette, removing the liquid with a pipette and lint-free wipes, and letting the sample dry face up (not tilted) caused negligible displacement or washing off of material, resulting in well preserved, distinctly stained sections. However, there was a limit of staining and washing steps before sample loss became difficult to avoid. For example, PAS staining successfully stained matrix components (Fig. 4g–i) but the intense staining and washing protocol led to visible disruption of section integrity (Fig. 4g). For staining procedures involving multiple staining and washing steps, agarose-embedding of sections added structural stability and improved section integrity and preservation. However, agarose-embedding is limited by non-specific binding to agarose by lectins (as observed in our study and reported by Bennke et al. 2013). Staining prior to embedding in cryogel may be considered to sidestep this problem, but limits the possibility of combining incompatible stains across consecutive slices and excludes aggregates embedded in situ.

Aggregate porosity

Optical porosity vs. calculated porosity Optical porosity of aggregate thin-sections ranged from 0.8 to 0.97 (void volume/total volume), and was found to be about 5–10% lower than calculated porosity (Alldredge and Gotschalk 1988). A possible cause was the integration of multiple layers of matter across the thickness of the section, leading to the omission of pore space and therefore underestimation of porosity. To minimize pore space omission, sections for measuring optical porosity should be cut as thinly as possible, i.e., 5–10 μm using our soft-embedding technique. Combining cryosectioning with optical sectioning (i.e., CLSM) improved resolution across depth, but was dependent on autofluorescence of solids or fluorescently stained substrates. Boundaries of aggregate thin-sections proved to be hard to determine due to loose connectivity and heterogeneous distribution of the solid fraction. We found that optical porosity varied by up to 50% depending on how the aggregate boundary was determined. This strongly suggested that a consistent approach for defining the section boundary was necessary. We compared various shapes for approximating the outer boundary of the sectioned aggregate (convex hull fittings, various ellipsoid fittings, polygons), and observed that the most robust approach for determining the outer boundary, and consequently to estimate the total area

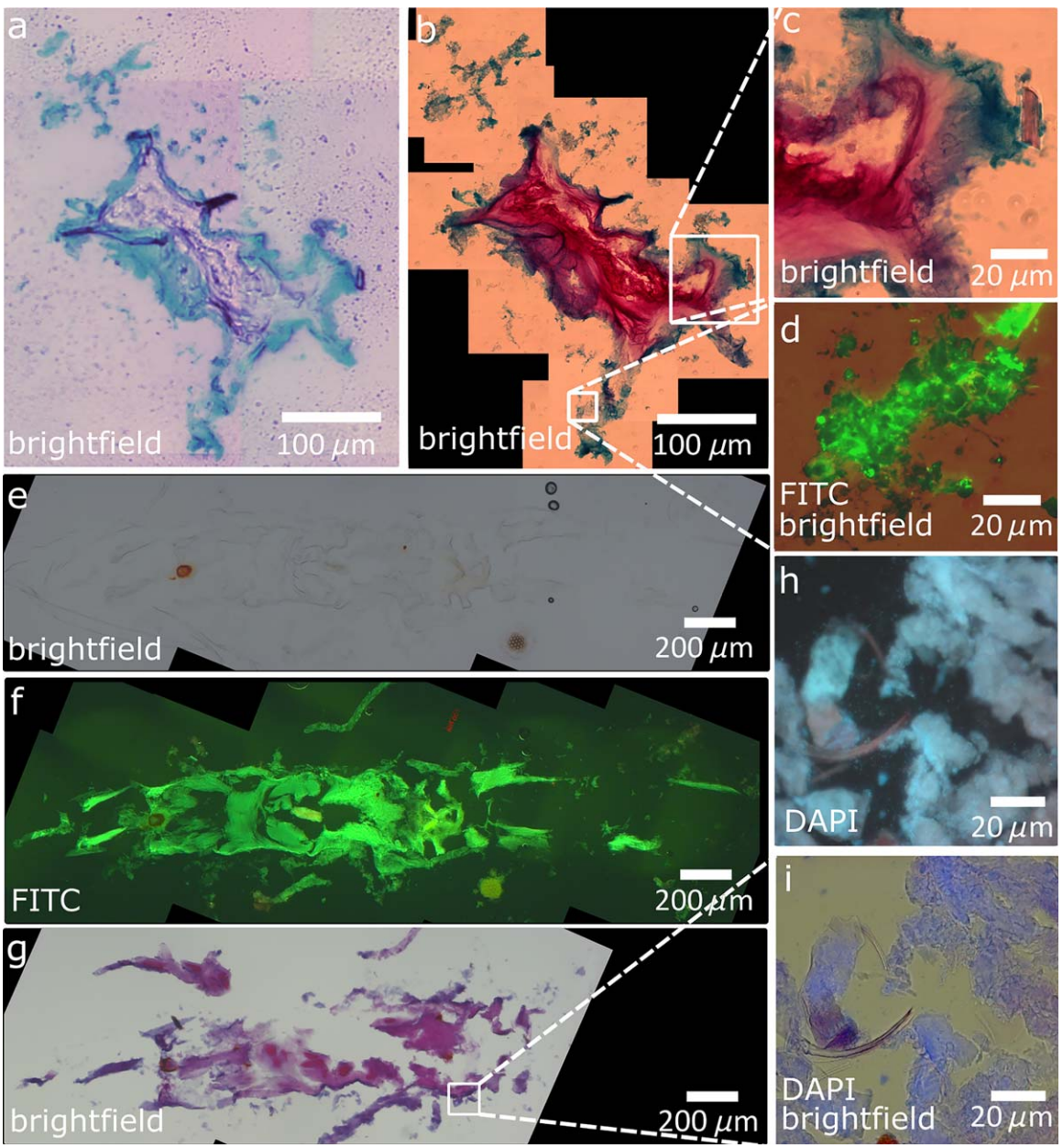

Fig. 4. Overview of matrix components in two separate thin-sections stained with selected dyes (section I **a**–**d**, section II **e**–**i**). (**a**) 10 μm-thick section I stained with Alcian Blue; (**b**) section I stained with Alcian Blue and Ruthenium Red; (**c**) close-up of section I stained with Alcian Blue and Ruthenium Red; (**d**) close-up of section I stained with Alcian Blue and FITC-ConA; (**e**) unstained 20 μm-thick section II imaged with brightfield microscopy; (**f**) section II imaged with fluorescence microscopy; (**g**) section II stained with PAS; (**h**) close-up of section II imaged with fluorescence microscopy; (**i**) close-up of section II imaged with fluorescence and brightfield microscopy.

of the section, was to fit an ellipse to the maximum aggregate width and height (Fig. 5). The same approach is used for measuring aggregate volume for porosity calculations (Alldredge and Gotschalk 1988) which is why this fitting resulted in the closest match to calculated porosity.

Pore size distribution between and across aggregate sections Optical porosity values were relatively constant across stacked aggregates sections, with mean values of 0.975 (SD $\pm$ 0.013) measured for the unstained aggregate. Porosity and pore size was much more variable across single sections where we generally observed regions with high porosity interspersed by regions of low porosity, with pore space being distributed more heterogeneously in aggregates collected in situ (Fig. 5a,b,d–f,h) compared with aggregates formed from diatom monocultures in the laboratory (Fig. 5c,g). Further, we observed large reductions in porosity down to 0.8454 (SD $\pm$ 0.040) in sections stained with Alcian Blue (Fig. 5g,h). Direct

assessment of thin-sections not only enabled the determination of porosity defined as the fraction of solid components to overall aggregate volume, but also of the effective porosity, i.e., porosity defined as the fraction of "non-void" components, including the EPS matrix, to aggregate volume. While Alcian Blue-staining reduced porosity by approximately 10%, we observed that Ruthenium Red reduced optical porosity by another 5–10%, but these observations can be expected to vary greatly depending on aggregate type and source. Thus, a combination of stains covering a broad range of polymers found in the marine snow matrix could potentially help to obtain more accurate estimates of effective aggregate porosity.

3D-reconstruction

3D reconstruction from cryosections highlighted the porous nature and heterogeneity of marine snow because of the possibility to examine aggregates from any chosen angle. The decrease in effective pore size by TEP became especially obvious when comparing the unstained with the Alcian Blue-stained reconstructed aggregate (Fig. 6). However, the patchy distribution of visible substrates and large amount of pore space complicated alignment of sections along the *z*-axis and stains with higher coverage (e.g., Alcian Blue) facilitated more precise alignment because of better cross-referencing between consecutive sections. To enable alignment independent of staining, we suggest introducing an external reference into the embedding matrix, which we so far have not achieved.

Visualization of aggregate colonizers

In addition to staining the aggregate matrix, we tested methods of staining bacteria in aggregate sections. Nucleic acid (DAPI) staining clearly visualized bacterial cells and their localization relative to autofluorescent and ConA-stained substrate, showing close bacteria-substrate associations (Figs. 3c,d, 7, 8).

Of the three FISH methods tested (mono-labeled FISH, multi-labeled FISH, and CARD-FISH), we determined multi-labeled FISH to be the most versatile method for staining selected clades of bacteria or archaea in soft-embedded sections: mono-labeled FISH (Fig. 8d) resulted in low fluorescent signal intensity and labeling success, possibly due to high autofluorescence of the samples (Fig. 3). CARD-FISH (Fig. 8c, e–g) yielded distinctive signals, but CARD-chemistry necessitates additional permeabilization and washing steps that can destabilize the integrity of the section and thus requires agarose-embedding of sections prior to CARD-FISH. Multi-labeled FISH combines the high signal intensity of CARD-FISH with the low amount of washing and sample handling of mono-labeled FISH (Fig. 8a,b). An additional advantage of multi-labeled FISH is the option of multiplexing several probes on the same section without the horseradish peroxidase inactivation necessary for CARD-FISH.

Following the FISH protocol without prior embedding of sections in 0.1% LE agarose led to some sections being lost in the process. Although not all sections were washed off, we observed that soft-embedding cannot provide sufficient structural support during FISH to guarantee sustained integrity of the sections, and recommend agarose-embedding before FISH.

Agarose-embedding has been found to limit the use of lectins in conjunction with CARD-FISH, as unspecific binding to agarose prohibits staining after CARD-FISH, but staining prior to embedding and CARD-FISH leads to severely reduced fluorescent signal intensity of the lectin stain. However, we did not observe any impact on the quality of the lectin stain following the mono- or multi-labeled FISH protocols. We attributed this to the lower number of washing steps compared to CARD-FISH which reduces loss of the label ligand as well as to the absence of protein-denaturing buffer solutions that are part of the CARD-FISH protocol. This endorses the use of multi-labeled FISH to be used in conjunction with EPS staining, as a protective agarose coating can be applied to the section after lectin staining but prior to multi-labeled FISH. Combining multi-labeled FISH and lectin staining in structurally preserved sections, we could see the accumulation of bacteria inside small channels in the polysaccharide matrix (Fig. 8a).

Discussion

In this study, we showed how combining soft-embedding with thin-sectioning of in situ collected aggregates provides insight into their physical structure and the distribution and diversity of microbial colonizers. A particular strength of this method lies in the minimal amount of active handling, particularly of aggregates embedded in situ in gel-filled collection cups. Without the possibility to analyze the composition and 3D structure of intact, non-embedded macro-aggregates, the degree of structural preservation during embedding and slicing cannot be assessed quantitatively. However, the consistent agreement of our findings regarding stainability, porosity, and composition to existing literature (as discussed in the "Assessment" section) strongly suggest minimal disturbance of aggregates during embedding and slicing. Good structural preservation during embedding is further supported by observations of natural aggregates collected with gel traps in previous studies (Ebersbach and Trull 2008; Laurenceau-Cornec et al. 2015; Wiedmann et al. 2016). Although some disturbance during sectioning and staining cannot be ruled out we have provided recommendations on how potential disturbances can be minimized (*see* "Assessment" for details). This is further supported by good alignment of consecutive sections enabling 3D reconstruction. The relative ease, lack of hazardous chemicals or specialized equipment, and low time expenditure for the embedding process make this method especially suited for ship- or field-based sampling. The compatibility with existing FISH protocols offers a previously unattainable spatial resolution of the distribution of microbial groups

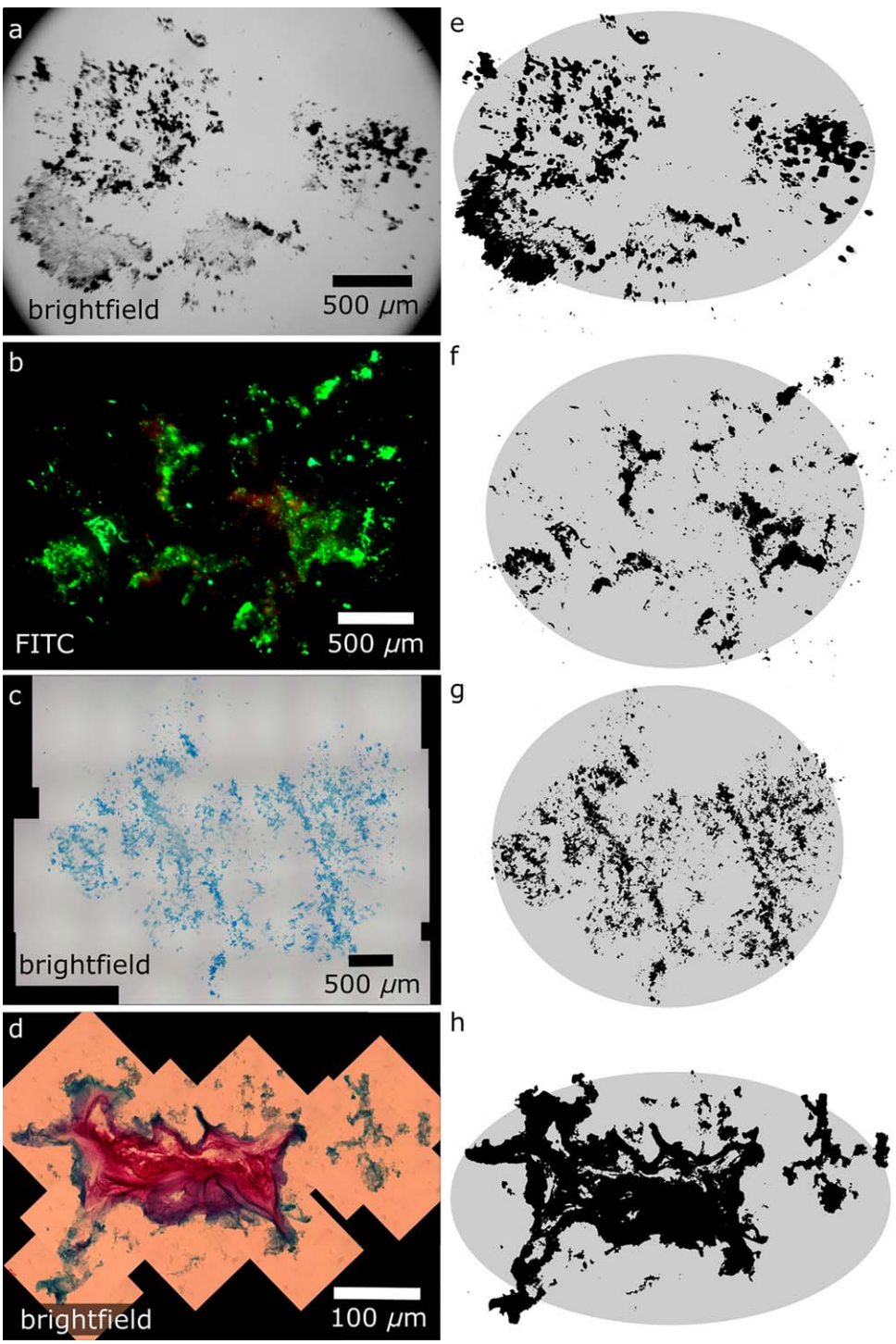

Fig. 5. Sections used to test optical porosity measurements. (**a**, **b**) Unstained 10 μm section of in situ collected aggregates; (**c**) Alcian Blue-stained 10 μm section of laboratory-formed *S. marinoi* aggregate; (**d**) Alcian Blue and Ruthenium Red-stained 10 μm section of in situ collected aggregate; (**e**–**h**) corresponding thresholded images used for measuring the area of solid or stained fractions (black) and ellipses fitted using the maximum width and height of the section to measure the total area of the section (overlay in gray).

within individual aggregates, with the added possibility of studying their co-localization with selected substrates of the aggregate matrix.

Preserving aggregate structure throughout staining and microscopy can shed light on attributes of marine snow that could so far not be examined because of disaggregation and

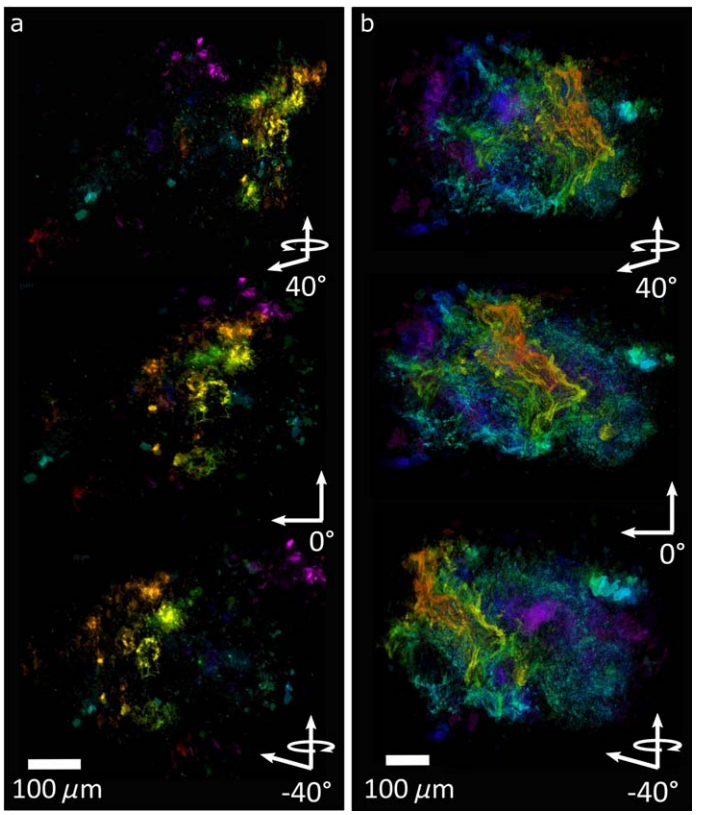

Fig. 6. 3D reconstruction of two 10 μm-sectioned aggregates based on (**a**) green autofluorescence and (**b**) Alcian Blue staining. Aggregates are pictured from three different angles, with a gradual change in color representing an increase in *z*-depth (frontback). Rotating video clips of both aggregates are available as Supporting Information.

structural disturbance during filtering. Several studies have explored the use of confocal laser scanning microscopy for the examination of structurally intact marine, riverine, and sludge aggregates (Thill et al. 1998; Neu 2000; Waite et al. 2000; Böckelmann et al. 2002). Compared to optical sectioning, embedding followed by physical sectioning can introduce sectioning artifacts (*see* "Assessment" section). However, optical sectioning also produces artifacts such as effects of self-shadowing, reduced fluorescent signal intensity with increasing scanning depth, bleaching of fluorescent signals, and limited working distance for larger samples (Dixon et al. 1991). Marine snow regularly reaches sizes of several millimeters, thereby limiting the resolution at which aggregates can be studied using Confocal Laser Scanning Microscopy alone. Embedding enables structurally preserved storage of samples, whereas optical sectioning requires immediate analysis as samples lack a supporting embedding matrix to retain structural integrity. Perhaps most importantly, we showed how physical sectioning offers the possibility of applying different stains to consecutive sections of the same aggregate to study the distribution of different matrix components across the aggregate (a form of pseudo-multiplexing), thus reducing limits imposed by overlapping color spectra of stains, fluorescent quenching, and stain incompatibility or interference. We do not consider optical section to be a feasible stand-alone method for analyzing in situ collected marine snow, but as we demonstrated in this study it can be a valuable complement to physical sectioning by increasing resolution across section depth, which is especially useful with respect to porosity measurements.

An alternative to the soft-embedding method presented here is embedding aggregates in hard resin (Leppard et al. 1996; Chu et al. 2004). Hard-embedding matrices support sectioning of ultra-thin slices (< 1 μm), which can be particularly useful for the investigation of sub-cellular structures and compartments (Heissenberger et al. 1996). Moreover, the resin matrix cannot be re-dissolved after polymerization, effecting high structural cohesion during washing and staining. Transport and long-term storage of hard-embedded samples is also more convenient, as it is not dependent on maintaining sub-zero temperatures. However, it is impossible

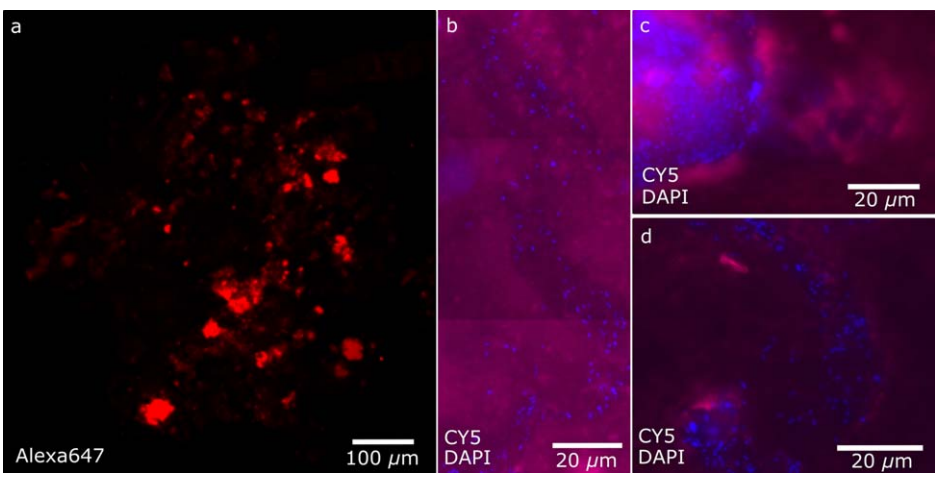

Fig. 7. (**a**) Section stained with Alexa647-ConA; (**b**–**d**) details showing ConA matrix (purple) with DAPI-stained bacteria embedded (blue).

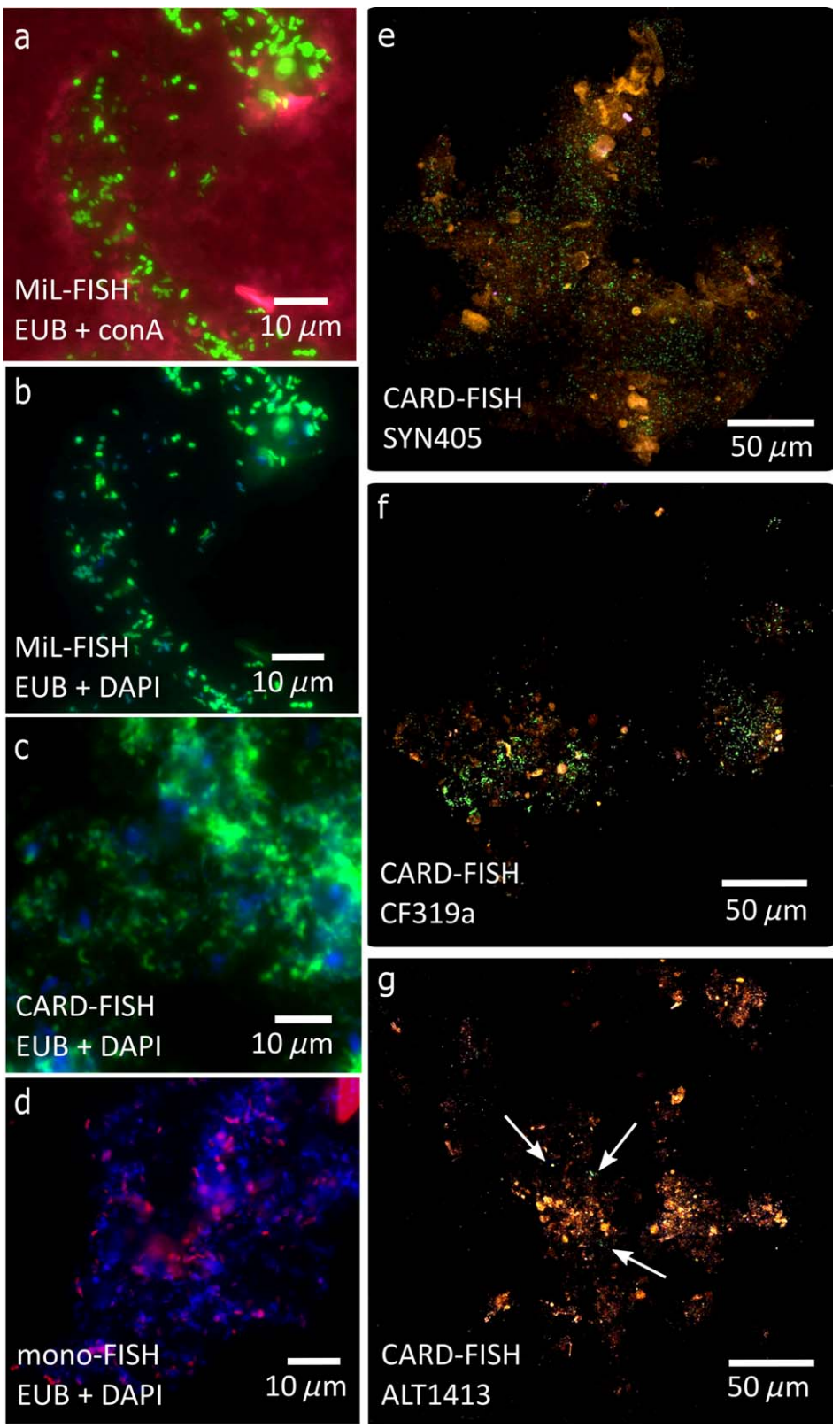

Fig. 8. FISH-probing of marine snow thin-sections. (**a**) EUB-labeled bacteria (green) embedded in channels inside the aggregate EPS matrix stained by conA (purple); (**b**–**d**) comparison of EUB labeling efficiency and fluorescent signal intensity for the three FISH methods used in this study: (**b**) MiL-FISH (green-fluorescent fluorophores); (**c**) CARD-FISH (green-fluorescent tyramides); (**d**) mono-FISH (red-fluorescent fluorophores); (**e**–**g**) thin-section from one in situ collected aggregate (phytoplankton autofluorescence shown in red) stained with probes for selected bacterial clades (green) using CARD-FISH: (**e**) *Synechococcus* spp.-specific probe; (**f**) *Bacteroidetes*-specific probe; (**g**) *Alteromonadales*-specific probe (arrows indicate localization of hardly visible FISH-stained bacteria). Rotating video clips of aggregate sections (**e**–**g**) are available as Supporting Information.

to equip sediment traps with hard resins to embed aggregates in situ. We consider direct fixation, washing, and embedding in situ to be one of the most substantial features of soft-embedding, as the absence of active handling prevents any risks of handling artifacts. The handling steps for soft-embedding of aggregates collected with a Marine Snow Catcher exclude the heating and complete dehydration that are needed for hard-embedding. The compatibility with FISH protocols furthermore enables taxonomic analysis of aggregate colonizers.

Practical applications of soft-embedding

Aggregate structure and porosity

By successfully staining the matrix of soft-embedded aggregate thin-sections using established staining protocols, we could visualize the spatial distribution of TEP and other EPS. By aligning consecutive sections along the *z*-axis we succeeded in rendering a 3D reconstruction of entire aggregates based on solid and Alcian Blue-stained fractions of the matrix. Aside from an increased appreciation of the aggregate-scale distribution of selected matrix fractions, 3D rendering enables clearer determination of aggregate boundaries in any direction than can be achieved by analyzing single sections. The current standard of quantifying TEP (and by extension EPS) developed by Passow and Alldredge (1995) involves filtering of organic material onto polycarbonate filters followed by staining and subsequent dissolution in sulfuric acid for spectrophotometric analysis, meaning no inferences can be made about the spatial distribution of TEP in aggregates.

In combination with spectrophotometric Alcian Blue assays (or lectin quantification assays as developed by Uthicke et al. 2009), and/or incubation experiments, examining the distribution and patchiness of EPS on a sub-aggregate level can advance our knowledge of what determines "stickiness" of aggregates and their components both during formation and disaggregation, and of the contribution by different EPS fractions to effective pore-space reduction. We also showed how applying several stains to cover a range of EPS could be used as a measure for "non-void," i.e., effective porosity, which can be used to approximate aggregate permeability. A separation into total and effective porosity can be useful to better understand mass transport of particulate and dissolved matter between aggregates and ambient water, as solid matter is restricted to being transported via actual pores, whereas fluids and gases can diffuse into and out of the aggregate matrix, which is of significance for colonization, nutrient release, oxygen supply, settling velocities, and mass fluxes.

Measuring the area of the solid or stainable fraction relative to the total area of thin-sections enabled us to estimate the optical porosity of sectioned aggregates and to give a spatially resolved structural description of intact marine snow. We do not suggest that the "optical porosity method" introduced here is superior to calculated porosity, as the inherent challenges (definition of the aggregate boundary, integration of matter across section depth) require further revision of this method. However, we regard it as a valuable complement to existing methods of calculating porosity, as direct visualization of matrix fractions and pore space can address questions that could so far not be resolved, including the effect of different solid and EPS fractions on porosity and pore distribution, and the variability of pore space across single sections. Furthermore, optical porosity can be estimated from singles aggregates, whereas calculating porosity according to Alldredge and Gotschalk (1988) requires averaging of values obtained from multiple aggregates due to methodological constraints. Analysis of pore distribution-connectivity across single sections together with alignment of consecutive sections and 3D reconstruction as demonstrated in this study, can enable detection of any channels through the aggregate matrix that could permit advective flow (i.e., channels that are connected to the outside of the aggregate and have a diameter greater than the Kolmogorov length scale of 5 μm, below which advection is drastically limited by viscosity). Exploring the presence and extent of advective flow remains a key goal, as advection has the potential to influence metabolic processes inside marine snow through influx of oxygenated water that reduces the occurrence or increases the patchiness of processes other than aerobic respiration (e.g., denitrification).

Microbial colonization and taxonomic diversity

Because of the preserved structure of embedded aggregates, we could spatially resolve the distribution of microbial colonizers inside individual aggregates. We consider this an important step toward exploring microbial colonization of marine snow in situ which can help resolve many outstanding questions about the colonization and succession dynamics on settling aggregates. Chemotactic, pelagic bacteria have been shown to be highly successful at seeking out small-scale nutrient patches like diatom cells or chains (Stocker et al. 2008; Smriga et al. 2016) and settling particles, which were newly colonized on scales of minutes to hours (Kiørboe et al. 2002, 2003; Grossart et al. 2003, 2006). Because of the dynamic aggregation and disaggregation of marine aggregates it is particularly hard to study in situ bacterial colonization and succession patterns. Often, such studies have been restricted to laboratory model systems (Datta et al. 2016) or inferences made from comparing community composition of free-living and particle-attached bacteria using filtered size-fractions (e.g., Mestre et al. 2017). Unfortunately, taxonomic composition of filter fractions has been shown to deviate notably from that of non-fractionated samples (Craig 1986; Padilla et al. 2015). In situ gel-embedding of marine aggregates sidesteps this issue as aggregates can be picked selectively from the gel to analyze their microbial composition, e.g., using FISH (Thiele et al. 2015). Thin-sectioning of embedded aggregates further allows high resolution studies of microbial colonization processes and dynamics in relation to small-scale aggregate structure and composition.

With preserved spatial structure, we showed the accumulation of bacteria inside small channels in the polysaccharide matrix. These channels could be formed through hydrolysis of the substrate by colonizing bacteria, or during aggregation and direct advective and diffusive flow of water carrying microorganisms through the aggregate matrix. Analyzing the localization of microbial groups or clusters inside aggregates over water depth and/or time could provide a way to study the respective importance or dominance of the bacterial community originally present during aggregate formation with that of bacteria attaching to (or being scavenged by) the aggregates during settling. Imaging of bacterial clades co-localized with substrates or degradation products also presents a way to directly visualize microbe–substrate interactions and complement current techniques used to infer microbial activity such as tracer addition to incubation experiments, transcriptomics, or single-cell uptake measurements.

Marine carbon fluxes and closing statement

Collecting and embedding aggregates in situ using drifting sediment traps not only minimizes active handling but presents a new and exciting possibility to study the micro-scale structure, composition and diversity of the aggregate matrix and aggregate colonizers in combination with particle characteristics, biogeochemical fluxes, and molecular methods applied to sediment trap material (e.g., DNA/RNA extraction). We consider this an important step toward understanding the ecology and connectivity of the pelagic zone with strong potential to open up new possibilities to research the microbial processes controlling the biological carbon pump and recycling of organic matter in the water column.

References

Alldredge, A. L., and C. Gotschalk. 1988. In situ settling behavior of marine snow. Limnol. Oceanogr. **33**: 339–351. doi:10.4319/lo.1988.33.3.0339

Alldredge, A. L., and M. W. Silver. 1988. Characteristics, dynamics and significance of marine snow. Prog. Oceanogr. **20**: 41–82. doi:10.1016/0079-6611(88)90053-5

Alldredge, A. L., and C. C. Gotschalk. 1990. The relative contribution of marine snow of different origins to biological processes in coastal waters. Cont. Shelf Res. **10**: 41–58. doi:10.1016/0278-4343(90)90034-J

Alldredge, A. L., U. Passow, and B. E. Logan. 1993. The abundance and significance of a class of large, transparent organic particles in the ocean. Deep-Sea Res. Part I **40**: 1131–1140. doi:10.1016/0967-0637(93)90129-Q

Amann, R. I., B. J. Binder, R. J. Olson, S. W. Chisholm, R. Devereux, and D. A. Stahl. 1990. Combination of 16S RRNA-targeted oligonucleotide probes with flow cytometry for analyzing mixed microbial populations. Appl. Environ. Microbiol. **56**: 1919–1925.

Bennke, C. M., T. R. Neu, B. M. Fuchs, and R. Amann. 2013. Mapping glycoconjugate-mediated interactions of marine bacteroidetes with diatoms. Syst. Appl. Microbiol. **36**: 417–425. doi:10.1016/j.syapm.2013.05.002

Böckelmann, U., W. Manz, T. R. Neu, and U. Szewzyk. 2002. Investigation of lotic microbial aggregates by a combined technique of fluorescent in situ hybridization and lectin-binding-analysis. J. Microbiol. Methods **49**: 75–87. doi:10.1016/S0167-7012(01)00354-2

Cardona, A., and others. 2012. TrakEM2 software for neural circuit reconstruction. PLoS One **7**: e38011. doi:10.1371/journal.pone.0038011

Chu, C. P., D. J. Lee, and X. F. Peng. 2004. Structure of conditioned sludge flocs. Water Res. **38**: 2125–2134. doi:10.1016/j.watres.2004.02.003

Ciais, P., and others. 2014. Current systematic carbon-cycle observations and the need for implementing a policy-relevant carbon observing system. Biogeosciences **11**: 3547–3602. doi:10.5194/bg-11-3547-2014

Cisternas-Novoa, C., C. Lee, and A. Engel. 2015. Transparent exopolymer particles (TEP) and Coomassie stainable particles (CSP): Differences between their origin and vertical distributions in the ocean. Mar. Chem. **175**: 56–71. doi:10.1016/j.marchem.2015.03.009 doi:10.1016/j.marchem.2015.03.009

D'Ambrosio, L., K. Ziervogel, B. MacGregor, A. Teske, and C. Arnosti. 2014. Composition and enzymatic function of particle-associated and free-living bacteria: A coastal/offshore comparison. ISME J. **8**: 2167–2179. doi:10.1038/ismej.2014.67

Datta, M. S., E. Sliwerska, J. Gore, M. F. Polz, and O. X. Cordero. 2016. Microbial interactions lead to rapid micro-scale successions on model marine particles. Nat. Commun. **7**: 11965. doi:10.1038/ncomms11965

DeLong, E. F., D. G. Franks, and A. L. Alldredge. 1993. Phylogenetic diversity of aggregate-attached vs. free-living marine bacterial assemblages. Limnol. Oceanogr. **38**: 924–934. doi:10.4319/lo.1993.38.5.0924

Dixon, A. E., S. Damaskinos, and M. R. Atkinson. 1991. A scanning confocal microscope for transmission and reflection imaging. Nature **351**: 551–553. doi:10.1038/351551a0

Ebersbach, F., and T. W. Trull. 2008. Sinking particle properties from polyacrylamide gels during the Kerguelen Ocean and Plateau compared Study (KEOPS): Zooplankton control of carbon export in an area of persistent natural iron inputs in the Southern Ocean. Limnol. Oceanogr. **53**: 212–224. doi:10.4319/lo.2008.53.1.0212

Grossart, H. P., T. Kiørboe, K. Tang, and H. Ploug. 2003. Bacterial colonization of particles: Growth and interactions. Appl. Environ. Microbiol. **69**: 3500–3509. doi:10.1128/AEM.69.6.3500-3509.2003

Grossart, H. P., T. Kirboe, K. W. Tang, M. Allgaier, E. M. Yam, and H. Ploug. 2006. Interactions between marine snow and heterotrophic bacteria: Aggregate formation and microbial dynamics. Aquat. Microb. Ecol. **42**: 19–26. doi:10.3354/ame042019

Heissenberger, A., G. G. Leppard, and G. J. Herndl. 1996. Ultrastructure of marine snow. II. Microbiological considerations. Mar. Ecol. Prog. Ser. **135**: 299–308. doi:10.3354/meps135299

Holloway, C. F., and J. P. Cowen. 1997. Development of a scanning confocal laser microscopic technique to examine the structure and composition of marine snow. Limnol. Oceanogr. **42**: 1340–1352. doi:10.4319/lo.1997.42.6.1340

Honjo, S., S. J. Manganini, R. A. Krishfield, and R. Francois. 2008. Particulate organic carbon fluxes to the ocean interior and factors controlling the biological pump: A synthesis of global sediment trap programs since 1983. Prog. Oceanogr. **76**: 217–285. doi:10.1016/j.pocean.2007.11.003

IPCC. 2013. Climate change 2013: The Physical Science Basis. 1535 pp. *In* T. F. Stocker, D. Qin, G.-K. Plattner, and others [eds.], Contribution of Working Group I to the Fifth Assessment Report of the Intergovernmental Panel on Climate Change. Cambridge University Press, Cambridge, United Kingdom and New York, NY, USA, doi: 10.1017/CB09781107415324

Iversen, M. H., and H. Ploug. 2010. Ballast minerals and the sinking carbon flux in the ocean: Carbon-specific respiration rates and sinking velocity of marine snow aggregates. Biogeosciences **7**: 2613–2624. doi:10.5194/bg-7-2613-2010

Iversen, M. H., and H. Ploug. 2013. Temperature effects on carbon-specific respiration rate and sinking velocity of diatom aggregates – potential implications for deep ocean export processes. Biogeosciences **10**: 4073–4085. doi:10.5194/bg-10-4073-2013 doi:10.5194/bg-10-4073-2013

Kiørboe, T., H. P. Grossart, H. Ploug, and K. Tang. 2002. Mechanisms and rates of bacterial colonization of sinking aggregates. Appl. Environ. Microbiol. **68**: 3996–4006. doi: 10.1128/AEM.68.8.3996-4006.2002

Kiørboe, T., K. W. Tang, H. P. Grossart, and H. Ploug. 2003. Dynamics of microbial communities on marine snow aggregates: Colonization, growth, detachment, and grazing mortality of attached bacteria. Appl. Environ. Microbiol. **69**: 3036–3047. doi:10.1128/AEM.69.6.3036-3047.2003

Krupke, A., L. R. Hmelo, J. E. Ossolinski, T. J. Mincer, and B. A. S. Van Mooy. 2016. Quorum sensing plays a complex role in regulating the enzyme hydrolysis activity of microbes associated with sinking particles in the ocean. Front. Mar. Sci. **3**: 55. doi:10.3389/fmars.2016.00055

Laurenceau-Cornec, E. C., and others. 2015. The relative importance of phytoplankton aggregates and zooplankton fecal pellets to carbon export: Insights from free-drifting sediment trap deployments in naturally iron-fertilised waters near the Kerguelen Plateau. Biogeosciences **12**: 1007–1027. doi:10.5194/bg-12-1007-2015

Leppard, G. G., A. Heissenberger, and G. J. Herndl. 1996. Ultrastructure of marine snow. I. Transmission electron microscopy methodology. Mar. Ecol. Prog. Ser. **135**: 289–298. doi:10.3354/meps135289

Long, R., and F. Azam. 1996. Abundant protein-containing particles in the sea. Aquat. Microb. Ecol. **10** (June): 213–221. doi:10.3354/ame010213

Luef, B., T. R. Neu, and P. Peduzzi. 2009*a*. Imaging and quantifying virus fluorescence signals on aquatic aggregates: A new method and its implication for aquatic microbial ecology. FEMS Microbiol. Ecol. **68**: 372–380. doi:10.1111/j.1574-6941.2009.00675.x

Luef, B., T. R. Neu, I. Zweimüller, and P. Peduzzi. 2009b. Structure and composition of aggregates in two large European rivers, based on confocal laser scanning microscopy and image and statistical analyses. Appl. Environ. Microbiol. **75**: 5952–5962. doi:10.1128/AEM.00186-09

Lundsgaard, C. 1995. Use of a high viscosity medium in studies of aggregates, p. 141–152. *In* S. Floderus, A.-S. Heisakanen, M. Oleson, and P. Wassman [eds.], Sediment trap studies in the Nordic countries 3. Proceedings of the Symposium on Seasonal Dynamics of Planktonic Ecosystems and Sedimentation in Coastal Nordic Waters.

Mari, X., U. Passow, C. Migon, A. B. Burd, and L. Legendre. 2017. Transparent exopolymer particles: Effects on carbon cycling in the ocean. Prog. Oceanogr. **151** (February): 13–37. doi:10.1016/j.pocean.2016.11.002

McSwain, B. S., R. L. Irvine, M. Hausner, and P. A. Wilderer. 2005. Composition and distribution of extracellular polymeric substances in aerobic flocs and granular sludge. Appl. Environ. Microbiol. **71**: 1051–1057. doi:10.1128/AEM.71.2.1051-1057.2005

Mestre, M., E. Borrull, M. Montserrat Sala, and J. M. Gasol. 2017. Patterns of bacterial diversity in the marine planktonic particulate matter continuum. ISME J. **11**: 999–1010. doi:10.1038/ismej.2016.166

Neu, T. R. 2000. In situ cell and glycoconjugate distribution in river snow studied by confocal laser scanning microscopy. Aquat. Microb. Ecol. **21**: 85–95. doi:10.3354/ame021085

Neu, T., G. D. Swerhone, and J. R. Lawrence. 2001. Assessment of lectin-binding analysis for in situ detection of glycoconjugates in biofilm systems. Microbiology **147** (Pt 2): 299–313. doi:10.1099/00221287-147-2-299

Padilla, C. C., S. Ganesh, S. Gantt, A. Huhman, D. J. Parris, N. Sarode, and F. J. Stewart. 2015. Standard filtration practices may significantly distort planktonic microbial diversity estimates. Front. Microbiol. **6**: 547. doi:10.3389/fmicb.2015.00547

Passow, U., and A. L. Alldredge. 1995. A dye-binding assay for the spectrophotometric measurement of transparent exopolymer particles (TEP). Limnol. Oceanogr. **40**: 1326–1335. doi:10.4319/lo.1995.40.7.1326

Passow, U., and C. A. Carlson. 2012. The biological carbon pump in a high CO2 world. Mar. Ecol. Prog. Ser. **470**: 249–271. doi:10.3354/meps09985

Pernthaler, A., J. Pernthaler, and R. Amann. 2002. Fluorescence in situ hybridization and catalyzed reporter

deposition for the identification of marine bacteria. Appl. Environ. Microbiol. **68**: 3094–3101. doi:10.1128/AEM.68.6.3094-3101.2002

Ploug, H., and H.-P. Grossart. 2000. Bacterial growth and grazing on diatom aggregates: Respiratory carbon turnover as a function of aggregate size and sinking velocity. Limnol. Oceanogr. **45**: 1467–1475. doi:10.4319/lo.2000.45.7.1467

Ploug, H., M. H. Iversen, and G. Fischer. 2008. Ballast, sinking velocity, and apparent diffusivity within marine snow and zooplankton fecal pellets: Implications for substrate turnover by attached bacteria. Limnol. Oceanogr. **53**: 1878–1886. doi:10.4319/lo.2008.53.5.1878

Ploug, H., and U. Passow. 2007. Direct measurement of diffusivity within diatom aggregates containing transparent exopolymer particles. Limnol. Oceanogr. **52**: 1–6. doi:10.4319/lo.2007.52.1.0001

Ransom, B., K. F. Shea, P. J. Burkett, R. H. Bennett, and R. Baerwald. 1998. Comparison of pelagic and nepheloid layer marine snow: Implications for carbon cycling. Mar. Geol. **150**: 39–50. doi:10.1016/S0025-3227(98)00052-8

Riley, J. S., R. Sanders, C. Marsay, F. A. C. Le Moigne, E. P. Achterberg, and A. J. Poulton. 2012. The relative contribution of fast and slow sinking particles to ocean carbon export. Global Biogeochem. Cycles **26**: GB1026. doi:10.1029/2011GB004085

Saalfeld, S., A. Cardona, V. Hartenstein, and P. Tomančák. 2010. As-rigid-as-possible mosaicking and serial section registration of large ssTEM datasets. Bioinformatics **26**: i57–i63. doi:10.1093/bioinformatics/btq219

Saalfeld, S., R. Fetter, A. Cardona, and P. Tomancak. 2012. Elastic volume reconstruction from series of ultra-thin microscopy sections. Nat. Methods **9**: 717–720. doi:10.1038/nmeth.2072

Schimak, M. P., M. Kleiner, S. Wetzel, M. Liebeke, N. Dubilier, and B. M. Fuchs. 2015. MiL-FISH: Multi-labelled oligonucleotides for fluorescence in situ hybridisation improve visualization of bacterial cells. Appl. Environ. Microbiol. **82**:62–70. doi:10.1128/AEM.02776-15

Schindelin, J., and others. 2012. Fiji: An open-source platform for biological-image analysis. Nat. Methods **9**: 676–682. doi:10.1038/nmeth.2019

Schindelin, J., C. T. Rueden, M. C. Hiner, and K. W. Eliceiri. 2015. The ImageJ ecosystem: An open platform for biomedical image analysis. Mol. Reprod. Dev. **82**: 518–529. doi:10.1002/mrd.22489

Schmid, B., J. Schindelin, A. Cardona, M. Longair, and M. Heisenberg. 2010. A high-level 3D visualization API for Java and ImageJ. BMC Bioinf. **11**: 274. doi:10.1186/1471-2105-11-274

Schneider, C. A., W. S. Rasband, and K. W. Eliceiri. 2012. NIH Image to ImageJ: 25 years of image analysis. Nat. Methods **9**: 671–675. doi:10.1038/nmeth.2089

Smith, D. C., M. Simon, A. L. Alldredge, and F. Azam. 1992. Intense hydrolytic enzyme activity on marine aggregates and implications for rapid particle dissolution. Nature **359**: 139–142. doi:10.1038/359139a0

Smriga, S., V. I. Fernandez, J. G. Mitchell, and R. Stocker. 2016. Chemotaxis toward phytoplankton drives organic matter partitioning among marine bacteria. Proc. Natl. Acad. Sci. USA **113**: 1576–1581. doi:10.1073/pnas.1512307113

Stocker, R., J. R. Seymour, A. Samadani, D. E. Hunt, and M. F. Polz. 2008. Rapid chemotactic response enables marine bacteria to exploit ephemeral microscale nutrient patches. Proc. Natl. Acad. Sci. USA **105**: 4209–4214. doi:10.1073/pnas.0709765105

Strathmann, M., J. Wingender, and H.-C. Flemming. 2002. Application of fluorescently labelled lectins for the visualization and biochemical characterization of polysaccharides in biofilms of Pseudomonas aeruginosa. J. Microbiol. Methods **50**: 237–248. doi:10.1016/S0167-7012(02)00032-5

Thiele, S., B. M. Fuchs, R. Amann, and M. H. Iversen. 2015. Colonization in the photic zone and subsequent changes during sinking determines bacterial community composition in marine snow. Appl. Environ. Microbiol. **81**: 1463–1471. doi:10.1128/AEM.02570-14

Thill, A., S. Veerapaneni, B. Simon, M. Wiesner, J. Y. Bottero, and D. Snidaro. 1998. Determination of structure of aggregates by confocal scanning laser microscopy. J. Colloid Interface Sci. **204**: 357–362. doi:10.1006/jcis.1998.5570

Tiessen, H., and J. W. B. Stewart. 1988. Light and electron microscopy of stained microaggregates: The role of organic matter and microbes in soil aggregation. Biogeochemistry **5**: 312–322. doi:10.1007/BF02180070

Tokuyasu, K. T. 1973. A technique for ultracryotomy of cell suspensions and tissues. J. Cell Biol. **57**: 551–565. doi:10.1083/jcb.57.2.551

Turner, J. T. 2015. Zooplankton fecal pellets, marine snow, phytodetritus and the ocean's biological pump. Prog. Oceanogr. **130**: 205–248. doi:10.1016/j.pocean.2014.08.005

Uthicke, S., L. Llewellyn, and F. Eder. 2009. Fluorescent lectin assay to quantify particulate marine polysaccharides on 96-well filtration plates. Limnol. Oceanogr.: Methods **7**: 449–458. doi:10.4319/lom.2009.7.449

Van der Jagt, H., C. Friese, J.-B. W. Stuut, G. Fischer, and M. H. Iversen. 2018. The ballasting effect of Saharan dust deposition on aggregate dynamics and carbon export: Aggregation, settling, and scavenging potential of marine snow. Limnol. Oceanogr. 9. doi:10.1002/lno.10779

Waite, A. M., R. J. Olson, H. G. Dam, and U. Passow. 1995. Sugar-containing compounds on the cell surfaces of marine diatoms measured using concanavalin a and flow cytometry. J. Phycol. **31**: 925–933. doi:10.1111/j.0022-3646.1995.00925.x

Waite, A. M., K. A. Safi, J. A. Hall, and S. D. Nodder. 2000. Mass sedimentation of picoplankton embedded in organic aggregates. Limnol. Oceanogr. **45**: 87–97. doi:10.4319/lo.2000.45.1.0087

Weissbrodt, D. G., T. R. Neu, U. Kuhlicke, Y. Rappaz, and C. Holliger. 2013. Assessment of bacterial and structural dynamics in aerobic granular biofilms. Front. Microbiol. **4**: 175. doi:10.3389/fmicb.2013.00175

Wiedmann, I., M. Reigstad, M. Marquardt, A. Vader, and T. M. Gabrielsen. 2016. Seasonality of vertical flux and sinking particle characteristics in an ice-free high arctic fjord—Different from subarctic fjords? J. Mar. Syst. **154(B)**: 192–205. doi:10.1016/j.jmarsys.2015.10.003

Wiedmann, I., M. Reigstad, A. Sundfjord, and S. Basedow. 2014. Potential drivers of sinking particle's size spectra and vertical flux of particulate organic carbon (POC): Turbulence, phytoplankton, and zooplankton. J. Geophys. Res. Oceans **119**: 6900–6917. doi:10.1002/2013JC009754

Woebken, D., B. M. Fuchs, M. M. M. Kuypers, and R. Amann. 2007. Potential interactions of particle-associated anammox bacteria with bacterial and archaeal partners in the Namibian upwelling system. Appl. Environ. Microbiol. **73**: 4648–4657. doi:10.1128/AEM.02774-06

Acknowledgments

We thank Bernhard Fuchs, Manuel Liebeke, Benedikt Geier, Mario Schimak, Jörg Wulf, and Andreas Ellrott for their support and advice developing the method presented in this paper. We appreciated the helpful comments provided by Helga van der Jagt and Allison Fong for editing this manuscript. This study was supported by the Helmholtz Association and the Alfred Wegener Institute for Polar and Marine Research (CMF, AR, AMW, MHI), the DFG-Research Center/Cluster of Excellence "The Ocean in the Earth System" (CMF, MHI), and the Max Planck Institute for Marine Microbiology (SM, ST). This publication is supported by the HGF Young Investigator Group SeaPump "Seasonal and regional food web interactions with the biological pump": VH-NG-1000.

Conflict of Interest

None declared.

Submitted 29 September 2017
Revised 01 February 2018; 13 March 2018
Accepted 16 March 2018

Associate editor: Gordon Taylor